Journal of Non-Crystalline Solids 481 (2018) 590–593

Contents lists available at ScienceDirect

Journal of Non-Crystalline Solids

journal homepage: www.elsevier.com/locate/jnoncrysol

Role of Mo addition on structure and magnetic properties of the $Fe_{85}Si_2B_8P_4Cu_1$ nanocrystalline alloy

Xingjie Jia[a], Yanhui Li[a], Guoqiang Xie[b], Tianlong Qi[a], Wei Zhang[a,*]

[a] Key Laboratory of Solidification Control and Digital Preparation Technology (Liaoning Province), School of Materials Science and Engineering, Dalian University of Technology, Dalian 116024, China

[b] School of Materials Science and Engineering, Harbin Institute of Technology (Shenzhen), Shenzhen 518055, China

ARTICLE INFO

Keywords:
Fe-based nanocrystalline alloys
Mo alloying
Amorphous-forming ability
Magnetic properties
Heating rate

ABSTRACT

The amorphous-forming ability (AFA), crystallization structure and magnetic properties of the melt-spun $Fe_{85-x}Si_2B_8P_4Cu_1Mo_x$ (x = 0–2) alloys were investigated. The addition of 1–2 at% Mo in the $Fe_{85}Si_2B_8P_4Cu_1$ alloy enhances the AFA with increasing the critical thickness for amorphous formation from ~14 to ~20 μm. The Mo alloying refines the microstructure and reduces the coercivity of the annealed alloys, and weakens the dependence of the coercivity on the heating rate, although it decreases the saturation magnetic flux density. After annealing under a low heating rate of 50 K/min, the average α-Fe grain size and coercivity of the $Fe_{84}Si_2B_8P_4Cu_1Mo_1$ alloy are ~25 nm and 23.9 A/m, respectively, which are lower than those of ~32 nm and 40.5 A/m for the base alloy. In addition, the mechanism related to the effects of Mo on the structure and magnetic properties was discussed in term of the crystallization activation energy.

1. Introduction

Soft magnetic materials have been widely applied as magnetic cores in inductors, sensors, and transformers. The demand for energy saving and device miniaturization drives the development of soft magnetic materials to the direction of high saturation magnetic flux density (B_s), high permeability, and low core loss. Among the developed soft magnetic materials, Fe-based nanocrystalline alloys with a structure of nano-sized α-Fe grains dispersing uniformly in the amorphous matrix have drawn considerable attention because of their low coercivity (H_c) and magnetostriction, high permeability, and low core loss in high frequency. However, the previously developed Fe-based nanocrystalline alloys typically in Fe-Si-B-Nb-Cu [1], Fe-M-B [2,3] and Fe-Co-M-B-Cu (M = Nb, Zr and Hf) [4,5] alloy systems usually contain a large amount of non-magnetic metal elements, which results in a significant decrease in B_s. Recently, new Fe-Si-B-P-Cu nanocrystalline alloys with high B_s of over 1.8 T were reported [6,7], while the relatively low amorphous forming ability (AFA) makes it difficult to produce amorphous precursor with stable quality in mass production. In addition, the microstructure and magnetic properties of the alloys show a strong sensitivity on the heating rate (H_r) for annealing [8]. The uniform and fine nanocrystalline structure and low H_c can only be obtained by annealing the amorphous precursor under a high H_r of 400 K/min. The relatively low AFA and demanding annealing process for obtaining good soft magnetic properties hinder the industrial production of the Fe-Si-B-P-Cu alloys.

We have found that addition of minor Mo effectively enhances the AFA of the Fe-based Fe-P-C-B alloys [9,10] due to its relatively large atomic radius and large negative enthalpies of mixing (ΔH^{mix}) with the components in the alloys [11–14]. Similar to the role of Nb in the Fe-Si-B-Nb-Cu alloys, adding Mo in the Fe-Si-B-P-Cu alloys is speculated to inhibit the growth of α-Fe grains during annealing, which is conducive to the formation of uniform and fine nanocrystalline structure and reduces the sensitivity of H_c of the alloy on the H_r. In this paper, with the aim of developing Fe-based nanocrystalline alloys with excellent magnetic properties and good manufacturability, the effects of minor Mo addition on the AFA, thermal stability, microstructure, and magnetic properties of the $Fe_{85}Si_2B_8P_4Cu_1$ alloy were investigated. The dependences of the microstructure and magnetic properties on the H_r were also studied and the relative mechanism was discussed in term of the crystallization activation energy.

2. Experimental procedure

Alloys ingots with nominal compositions of $Fe_{85-x}Si_2B_8P_4Cu_1Mo_x$ (x = 0–2) were prepared by alloying Fe (99.95 mass%), Si (99.999 mass %), B (99.9 mass%), Cu (99.99 mass%), Mo (99.95 mass%) and Fe_3P precursor (99.9 mass%) in an induction melting furnace under a high

* Corresponding author.
E-mail address: wzhang@dlut.edu.cn (W. Zhang).

https://doi.org/10.1016/j.jnoncrysol.2017.12.003
Received 12 October 2017; Received in revised form 29 November 2017; Accepted 2 December 2017
Available online 07 December 2017

purified argon atmosphere. The mass losses were < 0.2 mass%. Ribbon samples with a width of 1.5 mm and thicknesses of 14–25 μm were prepared by singer roller melt-spinning with linear velocities for copper wheel of 30–50 m/s in an argon atmosphere. The amorphous ribbons were subsequently annealed at different annealing temperatures (T_a) for 10 min in an argon atmosphere. The H_r to the required T_a are 10–400 K/min. The microstructure of the melt-spun and annealed samples were examined by X-ray diffraction (XRD, Bruker D8 Focus) with Cu *Kα* radiation and transmission electron microscopy (TEM, JEOL JEM-2010). The thermal properties of the melt-spun alloys were investigated in both isochronal and isothermal modes by differential scanning calorimetry (DSC, TA Instruments Q20). The isochronal DSC measurements were conducted from 298 to 873 K under heating rates increasing from 30 to 60 K/min by a step of 10 K/min. For the isothermal DSC measurements, the sample was first heated to a fixed temperature between 613 and 648 K, and then held isothermally for a certain period of time until the completion of crystallization. The B_s was measured with a vibrating sample magnetometer (VSM, Lake Shore 7410) under a maximum applied field of 800 kA/m. The H_c was measured with a dc *B-H* loop tracer (Linkjoin MATS-2010SD) using straight ribbons with a length of 60 mm under a maximum applied field of 4000 A/m.

3. Results and discussion

Fig. 1(a) shows the XRD patterns of the melt-spun $Fe_{85-x}Si_2B_8P_4Cu_1Mo_x$ (x = 0–2) alloy ribbons with different thickness

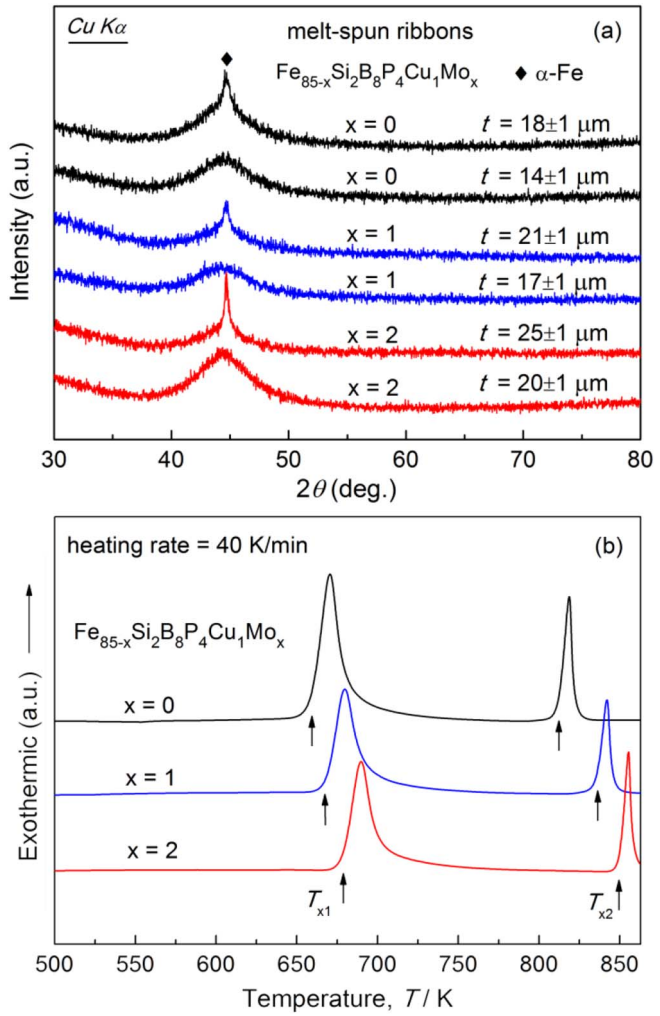

Fig. 1. XRD patterns (a) of melt-spun $Fe_{85-x}Si_2B_8P_4Cu_1Mo_x$ (x = 0–2) ribbons with different thickness and the DSC curves (b) of the amorphous alloys.

(*t*). For the alloy with x = 0, only a typical broad peak of amorphous structure was observed in the ribbon with *t* = ~14 μm, while the sharp diffraction peak matching α-Fe phase was found in the thicker ribbon, indicating that the critical thickness for amorphous formation (t_c) of the alloy is ~14 μm. According to the XRD results, the t_c of the alloys with x = 1 and 2 are ~17 and ~20 μm, respectively (see Fig. 1(a)). The correlation between the critical cooling rate (R_c) and t_c of the amorphous alloys can be roughly expressed as $R_c = 10/t_c^2$ [15]. The R_c of the alloy with x = 2 is estimated to be 2.5×10^6 K/s, which is half of that for the alloy with x = 0. The reduced R_c of the Mo-added alloys implies an effective enhancement of the AFA by adding minor Mo in the $Fe_{85}Si_2B_8P_4Cu_1$ alloy. Fig. 1(b) presents the DSC curves of the $Fe_{85-x}Si_2B_8P_4Cu_1Mo_x$ (x = 0–2) amorphous alloys. The curves all have two distinct exothermic peaks. With increasing the x from 0 to 2 at %, the onset temperature of the primary crystallization (T_{x1}) increases from 659 to 678 K, which reveals that the minor Mo addition enhances the thermal stability of the amorphous alloys. The temperature interval between the two crystallization peaks ($\Delta T = T_{x2}$-T_{x1}, T_{x2}: the onset temperature of the secondary crystallization) also widens from 154 to 172 K. It is known that the primary peak in the DSC curve of Fe-B-based amorphous alloys is associated to the precipitations of the α-Fe phase and the secondary according to non-ferromagnetic compounds like Fe-boride [6–8]. The large Δ*T* of the Fe-Si-B-P-Cu-Mo alloys facilitates the formation of the α-Fe nanocrystals without other non-ferromagnetic phases, which benefits to the achievement of good soft magnetic properties [16,17].

The addition of suitable alloying elements could enhance both AFA and thermal stability of the amorphous alloy in multi-component alloy systems [13,14]. For the Fe-Si-B-P-Cu-Mo alloys, the atomic radius of Mo (0.140 nm) is relatively larger than that of the other components, i.e., 0.132, 0.128, 0.127, 0.109, and 0.090 nm for Si, Cu, Fe, P, and B atom, respectively [11]. Appropriate Mo addition could produce an increased atomic packing degree of the liquid state by inducing the proper mismatch of atomic sizes, which is always associated with low free energy, and then facilitates the formation of amorphous alloys. The higher atomic packing degree also results in a higher density and viscosity, which could restrain the long-range diffusion of atoms, and then enhances the thermal stability of the amorphous alloys by retarding the precipitation of crystal phases [13]. In addition, Mo has large negative ΔH^{mix} with the components in the Fe-Si-B-P-Cu alloys, i.e., − 2, − 35, − 34 and − 53.5 kJ/mol for the Mo-Fe, Mo-Si, Mo-B and Mo-P atomic pairs, respectively [12]. The strong chemical affinities between the atomic pairs could also promote the atomic packing degree, which is also beneficial to the enhancement of AFA and thermal stability [13].

Fig. 2(a) shows the XRD patterns of the $Fe_{85-x}Si_2B_8P_4Cu_1Mo_x$ (x = 0–2) alloys annealed at 713 K for 10 min under a H_r of 400 K/min. It is seen that the single α-Fe phase was precipitated in all annealed alloys. The average size (*D*) of the α-Fe grains estimated by using Scherrer formula from the full width at half maximum of the (110) peak decreases from 20 to 18 nm with increasing x from 0 to 2 at%. The hysteresis loops of the annealed alloys are exhibited in Fig. 2(b). As the x increases from 0 to 2 at%, the H_c decreases from 7.7 to 5.3 A/m, and the B_s reduces from 1.84 to 1.70 T. The data were summarized in Table 1. The variations in H_c and B_s as a function of T_a of the alloys under a H_r of 400 K/min were investigated. As shown in Fig. 3, the H_c of the alloys all decrease gradually with T_a increasing from 653 to 698 K, and keep nearly a constant during a certain T_a range followed by a sharp lifting with further rise of T_a. Similar to the results at 713 K, the alloy with more Mo added always keeps a lower H_c at each T_a. The optimum T_a region (here artificially defined as the T_a region for H_c < 10.0 A/m) for the alloys with x = 0, 1, and 2 are ~30, ~60, and ~80 K, respectively. The B_s of the alloys increase with increasing T_a from 653 K to 668 K, and keep invariant in the T_a region of 668–788 K, namely same to the values at 713 K. The dependences of the magnetic properties on the H_r were studied as well. Fig. 4(a) shows the variation in H_c of the alloys annealed at 713 K for 10 min under the H_r of

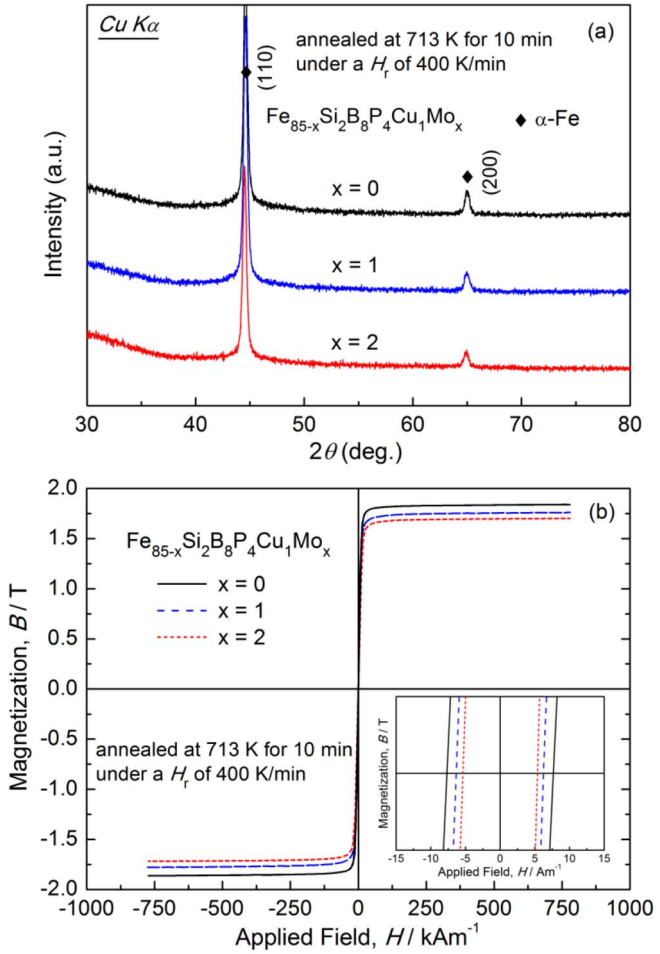

Fig. 2. XRD patterns (a) and hysteresis loops (b) of $Fe_{85-x}Si_2B_8P_4Cu_1Mo_x$ (x = 0–2) alloys annealed at 713 K for 10 min under a heating rate of 400 K/min.

Table 1
The thermal properties (T_{x1}, ΔT), critical thicknesses for amorphous formation (t_c), magnetic properties (B_s, H_c) and α-Fe grain size (D) of the $Fe_{85-x}Si_2B_8P_4Cu_1Mo_x$ (x = 0–2) alloys after annealing at 713 K for 10 min under heating rates of 400 and 50 K/min.

Alloys	T_{x1} (K)	ΔT (K)	t_c (μm)	400 K/min			50 K/min		
				B_s (T)	H_c (A/m)	D (nm)	B_s (T)	H_c (A/m)	D (nm)
x = 0	659	154	14	1.84	7.7	20	1.84	40.5	31
x = 1	668	168	17	1.76	6.2	19	1.75	23.9	25
x = 2	678	172	20	1.70	5.3	18	1.69	21.4	24

10–400 K/min. It is seen that although the H_c of the three alloys increase gradually with decreasing the H_r from 400 to 10 K/min, the H_c of the Mo-added alloys show obviously milder tendencies than that of the $Fe_{85}Si_2B_8P_4Cu_1$ alloy. After annealing under a low H_r of 50 K/min, the H_c of the alloys with x = 0, 1, and 2 are 40.5, 23.9, and 21.4 A/m, respectively. As listed in Table 1, the B_s of the alloys show no obvious change with the decrease of the H_r.

To well understand the weakened dependence of the H_c on H_r, the microstructure of the alloys annealed at 713 K under different H_r were investigated. The variation of D as a function of H_r is shown in Fig. 4(b). The dependence of D on H_r is quite similar to that of the H_c, i.e., although the D increases gradually with lowering the H_r from 400 to 10 K/min, the increase extent of the Mo-added alloys is lower than that of the base alloy, suggesting the Mo alloying is beneficial to the grain

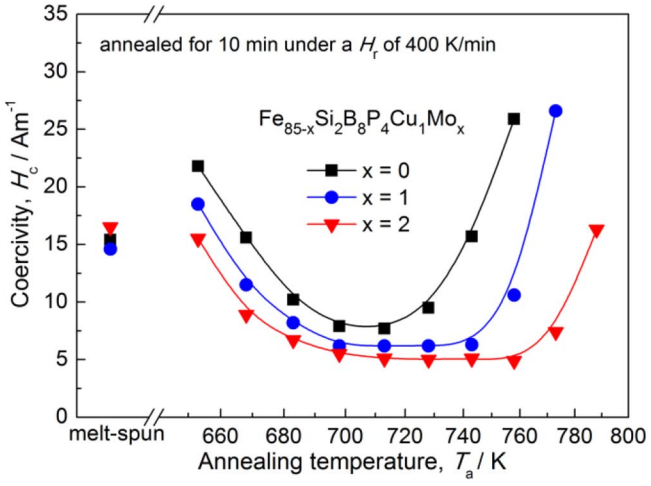

Fig. 3. Variation in coercivity as a function of annealing temperature for $Fe_{85-x}Si_2B_8P_4Cu_1Mo_x$ (x = 0–2) alloys.

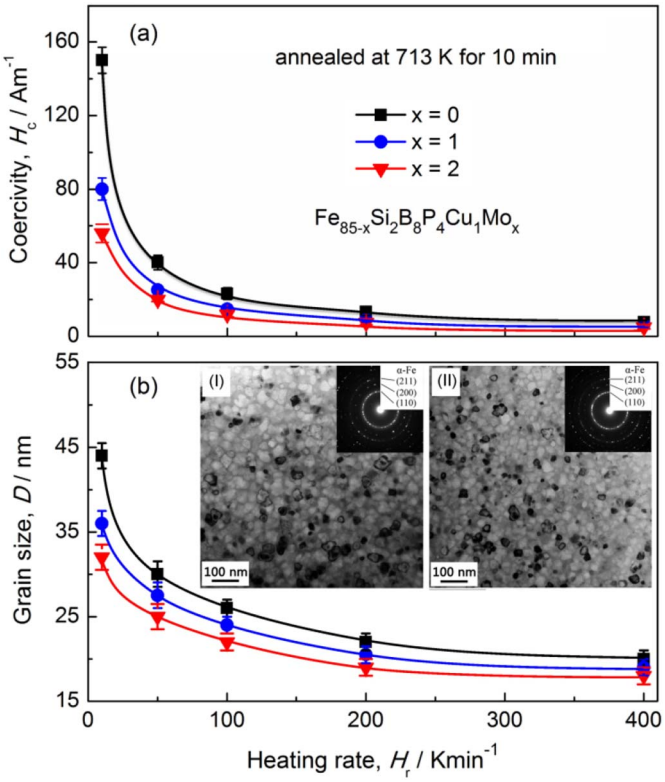

Fig. 4. Variations in coercivity (a) and α-Fe grain size (b) as a function of heating rate for $Fe_{85-x}Si_2B_8P_4Cu_1Mo_x$ (x = 0–2) alloys. The insets are the bright-field TEM images and selected area electron diffraction patterns of the $Fe_{85}Si_2B_8P_4Cu_1$ (I) and $Fe_{84}Si_2B_8P_4Cu_1Mo_1$ alloys (II) annealed at 713 K for 10 min under a heating rate of 50 K/min.

refinement. The microstructure of the $Fe_{85}Si_2B_8P_4Cu_1$ and $Fe_{84}Si_2B_8P_4Cu_1Mo_1$ alloys annealed under a low H_r of 50 K/min were examined by TEM. As shown in the insets of Fig. 4(b), both the alloys show typical nanocrystalline structure with α-Fe grains (identified by the selected area electron diffraction patterns) dispersing in the amorphous matrix. For the alloy with x = 0, the D of the α-Fe grains mainly distributes in the range of 10–55 nm and the average value is ~32 nm. In comparison, the α-Fe phase in the alloy with x = 1 shows a smaller D of ~25 nm with more uniform size distribution of 15–38 nm. It is then confirmed that Mo addition in the $Fe_{85}Si_2B_8P_4Cu_1$ alloy is beneficial to the formation of uniform nanocrystalline structure with fine α-Fe grains. According to the random anisotropy model, the intergranular

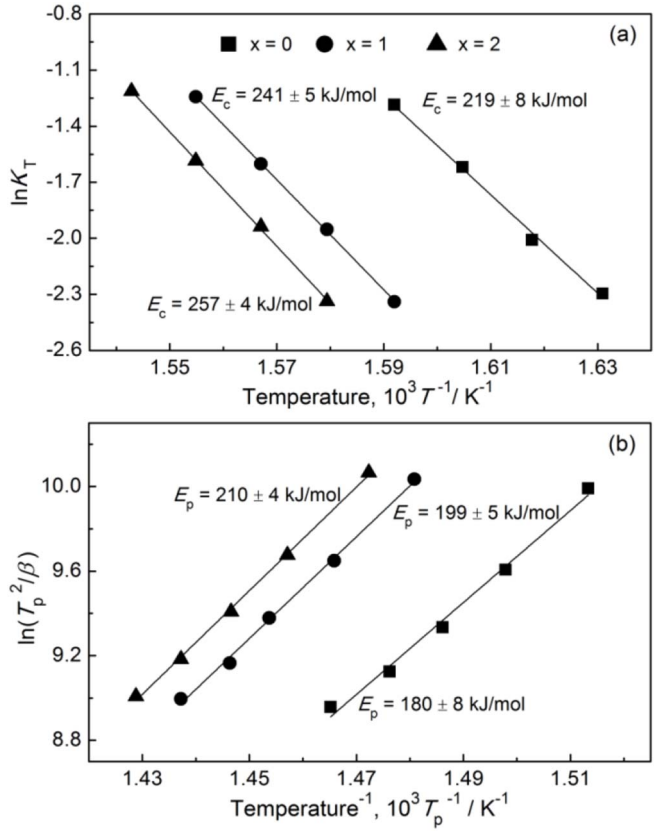

Fig. 5. Arrhenius plots for the isothermal crystallization at different temperatures (a) and Kissinger plots for peak temperature of the primary crystallization (b) of $Fe_{85-x}Si_2B_8P_4Cu_1Mo_x$ (x = 0–2) amorphous alloys.

exchange coupling between the α-Fe grains could minimize the effect of the magneto-crystalline anisotropy when the D of the α-Fe grains is smaller than the exchange-coupled length (30–40 nm). In this condition, the H_c of the nanocrystalline soft magnetic alloys are almost proportional to D^6 [18]. The Mo addition in the $Fe_{85}Si_2B_8P_4Cu_1$ alloy refines the α-Fe grains size, and thus lowers the H_c of nanocrystalline alloy. On the other hand, the substitution of nonmagnetic Mo for Fe results in a reduction of the volume fraction of the α-Fe phase in the annealed alloys, which leads to the decrease of B_s [19].

To clarify the mechanism of the effects of Mo on refining the microstructure, the crystallization kinetics of the $Fe_{85-x}Si_2B_8P_4Cu_1Mo_x$ (x = 0–2) amorphous alloys were studied under both isothermal and isochronal modes. Under isothermal conditions, the apparent activation energy (E_c) of the crystallization process can be calculated by using the Arrhenius-type equation [20]: $K_T = K_0\exp(-E_c/RT)$, where K_T is the temperature-dependent kinetic constant which can be calculated by the Johnson-Mehl-Avrami equation [21–24], K_0 is a constant, R is the gas constant and T is the isothermal temperature. The Arrhenius plots lnK_T vs. $1/T$ were drawn in Fig. 5(a), and the E_c were calculated by linear fitting the slope of the plots, which are 219 ± 8, 241 ± 5, and 257 ± 4 kJ/mol for the alloys with x = 0, 1, and 2, respectively. For the isochronal crystallization processes, the activation energy E_p for the growth of crystal phase could be calculated through the Kissinger method [25]: $\ln(T_p^2/\beta) = E_p/RT_p$ + Constant, where β is the heating rate, and T_p is the peak temperature for the primary crystallization peak in the DSC curves under different heating rates. As shown in Fig. 5(b), the E_p determined by linear fitting the Kissinger plots were 180 ± 8, 199 ± 5, and 210 ± 4 kJ/mol for the alloys with x = 0, 1, and 2, respectively. The increased crystallization activation energy (E_c and E_p) of the Mo-added alloys suggests that Mo addition could provide a larger energy barrier for the growth of the α-Fe grains as compared with the $Fe_{85}Si_2B_8P_4Cu_1$ alloy. The large energy barrier is presumably attributed to the large atomic radius of Mo element, and large negative ΔH^{mix} between the Mo and other components in the alloys. Accordingly, the growth of the α-Fe grains can be inhibited effectively, which results in the uniform nanocrystalline structure with fine α-Fe grains.

4. Conclusions

The effects of Mo addition on the AFA, thermal stability, microstructure, and magnetic properties of the $Fe_{85}Si_2B_8P_4Cu_1$ alloy were investigated. The detailed conclusions can be summarized as below:

(1) The Mo addition in the $Fe_{85}Si_2B_8P_4Cu_1$ alloy enhances the AFA and thermal stability. As the Mo content increases from 0 to 2 at%, the t_c, T_{x1}, and ΔT of the amorphous alloys increase from 14 μm, 659 K, and 154 K to 20 μm, 678 K, and 172 K, respectively.
(2) The Mo-containing alloys show improved magnetic softness and wide optimum T_a region as compared with the base alloy. The $Fe_{84}Si_2B_8P_4Cu_1Mo_1$ alloy exhibits a low H_c of 6.2 A/m and a high B_s of 1.76 T in a wide T_a region of ~60 K under a H_r of 400 K/min.
(3) The Mo alloying weakens the dependence of the microstructure and magnetic properties of the alloys on the H_r. After annealing under a low H_r of 50 K/min, the $Fe_{84}Si_2B_8P_4Cu_1Mo_1$ alloy possesses more uniform and finer nanocrystalline structure with an α-Fe grain size of ~25 nm, lower H_c of 23.9 A/m, and B_s of 1.75 T compared with those of ~32 nm, 40.5 A/m, and 1.84 T for the base alloy.
(4) The increased crystallization activation energy of the Mo-added alloys reveals that the Mo could inhibit the growth of α-Fe grains during annealing, which is contributed to the fine nanocrystalline structure and improved magnetic softness.

Acknowledgement

This research was supported by the National Natural Science Foundation of China [Grant No. 51571047], the National Key Research and Development Program of China (Grant No. 2017YFB0903903), the Natural Science Foundation of Liaoning Province [Grant No. 201602184] and the Fundamental Research Funds for the Central Universities (DUT17ZD212, DUT17LAB10).

References

[1] Y. Yoshizawa, S. Oguma, K. Yamauchi, J. Appl. Phys. 64 (1988) 6044–6046.
[2] K. Suzuki, N. Kataoka, A. Inoue, A. Makino, T. Masumoto, Mater. Trans. JIM 31 (1990) 743–746.
[3] K. Suzuki, A. Makino, A. Inoue, T. Masumoto, J. Appl. Phys. 74 (1993) 3316–3322.
[4] M.A. Willard, D.E. Laughlin, M.E. McHenry, D. Thoma, K. Sickafus, J.O. Cross, V.G. Harris, J. Appl. Phys. 84 (1998) 6773–6777.
[5] M.A. Willard, M.Q. Haung, D.E. Laughlin, M.E. McHenry, J.O. Cross, V.G. Harris, C. Franchetti, J. Appl. Phys. 85 (1999) 4421–4423.
[6] A. Makino, IEEE Trans. Magn. 48 (2012) 1331–1335.
[7] A. Makino, T. Kubota, K. Yubuta, A. Inoue, A. Urata, H. Matsumoto, S. Yoshida, J. Appl. Phys. 109 (2011) 07A302.
[8] P. Sharma, X. Zhang, Y. Zhang, A. Makino, Scr. Mater. 95 (2015) 3–6.
[9] W. Zhang, X.J. Jia, Y.H. Li, J. Appl. Phys. 115 (2014) 17A768.
[10] W. Zhang, C.F. Fang, Y.H. Li, Scr. Mater. 69 (2013) 77–80.
[11] Japan. Inst. Metals, Metals Databook, Maruzen, (1983).
[12] A. Takeuchi, A. Inoue, Mater. Trans. JIM 46 (2005) 2817–2829.
[13] W.H. Wang, Prog. Mater. Sci. 52 (2007) 540–595.
[14] A. Inoue, Acta Mater. 48 (2000) 279–306.
[15] X.H. Lin, W.L. Johnson, J. Appl. Phys. 78 (1995) 6514–6519.
[16] B.L. Shen, H. Kimura, A. Inoue, Mater. Trans. 43 (2002) 589–592.
[17] R. Xiang, S.X. Zhou, B.S. Dong, Y.G. Wang, J. Mater. Sci. 26 (2015) 4091–4096.
[18] G. Herzer, IEEE Trans. Magn. 26 (1990) 1397–1402.
[19] Z. Xiang, A.D. Wang, C.L. Zhao, H. Men, X.M. Wang, C.T. Chang, D. Pan, J. Alloys Compd. 622 (2015) 1000–1004.
[20] M.G. Scott, P. Ramachandrarao, Mater. Sci. Eng. A 29 (1977) 137–144.
[21] W.A. Johnson, R.F. Mehl, Trans. Am. Inst. Mining Met. Engrs. 135 (1939) 416.
[22] M. Avrami, J. Chem. Phys. 7 (1939) 1103–1112.
[23] M. Avrami, J. Chem. Phys. 8 (1940) 212–224.
[24] M. Avrami, J. Chem. Phys. 9 (1941) 177–184.
[25] H.E. Kissinger, Anal. Chem. 29 (1957) 1702–1706.